Biology, Engineering and Medicine

Scientific Article

ISSN: 2399-9632

Pre-clinical demonstration of a rapid and non-contact method to quantify burn injury using attenuation of the optical coherence tomography signal

Dan P Popescu[1]*, Michael SD Smith[1] and Michael G Sowa[2]

[1]National Research Council of Canada, Medical Devices Research Center, Canada

[2]Kent Imaging, 804B 16th Ave SW, Calgary AB, T2R 0S9, Canada

Abstract

A porcine burn model was used to demonstrate the potential of using the attenuation of the optical coherence tomography signal as an indicator of the degree of burn injury. A swept-source optical coherence tomography system amenable to operating in burn trauma centers and in surgeries was designed and built in-house. A special design feature of our optical coherence tomography system is its large stand-off distance (272 mm) between the data collecting lens terminating the sample arm and the sample surface. This feature eliminates potential contact between patient and instrument, and thereby decreases the potential for infection through remote contamination. Four contact burn types, histologically confirmed to produce superficial, superficial-intermediate, deeper-intermediate and full thickness injuries, were investigated. Burn types and matching control sites were randomly placed over a predetermined grid. The burn injuries were restricted to under 1% of the total body surface area in order to minimize systemic effects and eliminate cross-talk between the measurement sites on the grid. At each grid location, the data was acquired very fast, amounting to total acquisition times of less than 3 seconds per data set, speeds practical for use in the high-stress environment characterizing burn trauma units. We used attenuation coefficients of optical coherence tomography signal in tissue as a summary parameter for burn injury determination. This simple parameter can be computed in real-time during the OCT acquisition sequence across the burn wound providing the clinician a real-time assessment of the degree of injury.

Introduction

Burn injuries can be life threatening or, at their very least, life altering. Accurate and early assessment of burn injuries improves outcomes as well as the functional recovery of the patient. One of the key facts to be established is if healing will require just appropriate wound care or surgery. For burn specialists it is indeed very easy to differentiate between superficial (first degree) and full-thickness (third degree) burns. Meanwhile, diagnosis becomes more challenging for classification of intermediate thickness also known as partial-thickness cases. The accuracy of the diagnosis is further challenged when it is made early in the post-burn period as the wound responds to the insult.

It is common knowledge that prognosis for burn injuries is critically dependent on the supply of blood to the wound. The burn depth also relates directly to its healing capacity. Superficial injuries, where the vascular supply to the dermis of the skin remains largely intact, generally heal with standard wound care. Meanwhile full thickness injuries, which destroy the vascular supply in the dermis, do not spontaneously heal and will require surgery. The question is what happens to the wounds between these two extremes? The outcomes of these partial thickness injuries are very difficult to predict, especially immediately postburn, and there are no objective methods to help in determining wound depth or healing potential of such injuries. Generally, a wait and see approach is adopted but this approach increases the infection risk, the chances for a thicker scar and also prolongs the pain associated with a healing wound. On the other hand, a hastened skin graft surgery could mean expensive over-treatment coming with a host of other potential complications. Therefore, a technology that can accurately predict the outcome of partial thickness burn wounds in the early post-burn period would dramatically improve the management of burn injuries by enabling prompt and appropriate treatment.

One current standard practice for burn severity determination is subjective clinical assessment of the burn wound. Nevertheless, experienced clinicians have demonstrated inaccurate diagnosis between deep and superficial partial thickness wounds burns approximately 35-50% of the time [1-3]. By convention, experts anatomically categorize the depth of a burn into four major groups: superficial (only the epidermis is injured), superficial partial thickness (papillary dermis), deep partial thickness burn (burn reaches the reticular dermis) and full thickness (injury affects the entire dermis and extends into the subcutaneous fat). Adding another degree of complexity is the fact that burns are generally heterogeneous, with appearance varying affected across the affected region. Additionally, burn wounds are dynamic injuries responding to the inflammatory cascade that the body mounts as a defense against the insult. Injuries, which can appear superficial at the outset can convert to non-viable full-thickness injuries within the first 72 h [3,4].

Thus, treatment decisions for any thermal injury depends upon the burn depth but inaccurate diagnosis translates into either treatment delays or unnecessary surgery. Providing a suitable treatment

Correspondence to: Dan P Popescu, National Research Council of Canada, Medical Devices Research Center, 435 Ellice Ave, Winnipeg MB, R3B 1Y6, Canada, E-mail: Dan.Popescu@nrc-cnrc.gc.ca

Received: March 25, 2019; **Accepted:** April 04, 2019; **Published:** April 10, 2019

immediately after the burn onset would be the ideal situation and this could be accomplished with an objective measure of burn wound viability early in the post-burn period. The current lack of such an objective method results in prolonged inpatient hospital stays or multiple outpatient visits required for clinicians to determine the burn progression. As inpatient burn management is extremely costly, therefore the safe triage of patients with viable wounds that do not require inpatient care or surgery would indeed significantly reduce the costs [5]. An objective measure of burn wound viability at the earliest stages would indeed allow for early determination of surgical vs non-surgical as well as inpatient *vs.* outpatient management. The demand for the development of an objective technology for burn assessment has resulted in the emergence of several techniques to assist in probing tissue viability. Some of these modalities provide macroscopic assessment of entire regions, while others cover only selected small areas.

Still considered the gold standard of burn assessment, punch biopsy has some very obvious drawbacks. Most importantly, the procedure is highly invasive causing discomfort and additional scarring. Since burn severity can vary greatly over a small area, punch biopsy can be very vulnerable to sampling errors. The process itself is very time-consuming and requires the presence of a pathologist for sample acquisition, sectioning, staining and diagnosis. Owing to these complications, punch biopsies are generally relied upon clinically.

Laser Doppler imaging (LDI) is currently the most widely used noninvasive optically-based burn assessment technique, with several commercial devices available. One advantage of LDI is that it can be performed non-invasively, with no physical contact with the patient. The laser energy emitted is harmless and a large area can be evaluated [6]. A fairly large body of literature on the subject of LDI speaks to the potential utility of the technology. However, LDI has its own drawbacks, some of them serious. The current commercial devices are expensive, large and difficult to position [7]. When counting the time required to position, calibrate, and scan, the whole measurement procedure can take several minutes, during which the patient must remain motionless to avoid artifacts which would render Doppler measurements useless. This indeed will place an additional burden on already anxious or shivering patients and on young children in particular, necessitating sedation. Full-field speckle imaging-based perfusion measurements can be made quicker but motion between the patient and instrument remains a serious confounding factor. Errors can also result due vasomotor reactivity and blood pooling in response to changes in ambient temperature, patient positioning and emotional states [8]. Conditions such as anemia, cellulitis, or peripheral vascular disease complicate the interpretation of LDI/Speckle blood flow maps. Also surface moisture, topical medications, as well as transparent dressings can alter LDI results [9]. In addition, tissue surface topology also makes recorded signals difficult to interpret. Neither Doppler nor speckle based flow measurement systems have met with widespread clinical acceptance due to these factors.

Videoangiography based on recording of fluorescence generated by injected indocyanine green (ICG) is a widely clinically accepted method to visualize perfusion. ICG is a non-toxic dye that is retained within the vasculature for several minutes after intravenous injection until its rapid clearance by the liver. ICG fluorescence angiography can also help with burn diagnosis. ICG absorbs and fluoresces within the near infrared spectrum, which has excellent skin penetration making deeper dermal vasculature visible when using this dye [10]. With ICG videoangiography the in and out-flow of the bolus dose of the dye throughout the underlying dermal vasculature can be visualized in real-time. From the video sequence, macroscopic maps of vascular circulation can be extracted. Its utility has been clearly demonstrated even in the presence of other microvascular pathologies, such as diabetes and heart failure [11]. The obvious drawback of ICG videoangiography is the need for intravascular dye injection, since sometimes ICG is associated with headache, pruritis, urticaria, diaphoresis, and the risk of life-threatening anaphylactic reaction [12]. Safety has not been well-established in pediatric, pregnant or lactating patients. Additionally, measurements obtained via ICG videoangiography are relative to normal skin controls, and anatomically equivalent regions of normal skin are not always available in burn subjects.

Another burn diagnostic method based on the variations of reflectance and/or absorption spectra produced by different degrees of injury is near-infrared spectroscopy (NIRS). It was demonstrated that NIRS differentiate between superficial partial and deep partial burns with an accuracy of 87% in animal models [13]. Near-infrared light can penetrate further into tissue than visible light, and relays information on several biochemical constituents in the dermis. The most relevant constituent for burn assessment is hemoglobin. The NIRS ability to differentiate between oxygenated and deoxygenated blood confers an advantage to this modality. Thus, rather than measure a parameter related to blood flow, NIRS identifies blood oxygen presence or the lack thereof. Moreover, it has been reported that NIRS has the potential to identify collagen damaged due to burn wounds [14]. Therefore, a possible path to enhance the predictive reliability of this method would be by using an NIRS instrument that could simultaneously probe oxyhemoglobin and de-oxyhemoglobin [15]. On the downside, NIRS scans may take several minutes to complete. In some configurations, for example point source-to-point detector devices, scanning requires physical contact with the wound thus causing discomfort and enhancing contamination potential. It had been shown that NIRS reliably differentiates superficial from full thickness burns in human subjects but is not specific enough to diagnose superficial partial from deep partial [16]. Finally, although allowing for a great diversity of system designs and data algorithms, there is also a distinct lack of standardization in NIRS instrumentation to this day. To date, NIRS methods have not been clinically adopted in the assessment of burns.

Various microscopy imaging methods, such as capillary videomicroscopy, orthogonal polarization spectral microscopy and reflection-mode confocal microscopy, can also be included amongst the methods used for burn diagnostics. All these microscopy imaging modalities share similar drawbacks: very small fields of view, time-consuming, requirement of special training both on the clinical and technical side, as well as small distances between the objective lens and patient thus increasing the potential for wound contamination.

Experimental setup

For this work we used a swept-source optical coherence tomography (OCT) prototype specially designed and built in-house. What sets our prototype apart from other OCT systems is the large distance between the investigated tissue and the exit aperture of the telecentric lens terminating the sample arm. This design of the sample arm allowed a working distance of 272 mm between the patient and lens surface during data collection. Meanwhile, all other OCT systems deployed in skin and burn studies have had reported stand-off distances of 25 mm or less. When utilized in a general clinical setting and specifically in burn wound assessment where infection control is paramount, our prototype would minimize the possibility of contact between patient and instrument. This greatly reduces the risk of infection through

incidental contact with the instrument. Our design also has a large collection area (i.e. field of view) of 8 cm × 8 cm, enabling it to survey larger wound areas without having to re-position the patient or the OCT system. This field of view is at least 10 times larger than collection areas reported for OCT systems deployed in similar studies.

Extensive details about our swept source OCT imaging system are provided in reference [17]. Briefly, the laser swept-source (HSL-series, SANTEC) used in the interferometer of this prototype had a central wavelength of 1545 nm, a 140 nm spectral range, an average output power of 14 mW, and a free-space axial resolution, measured at the full-width half-maximum (FWHM) of the autocorrelation function, of 12 μm. Its repetition rate was 20 kHz with a duty cycle of 85%. The source output was launched into a 2 × 2 coupler, which diverted 90% of the available power toward the sample arm and 10% into the reference arm. Both arms contained circulators to guide the light back-reflected from the sample and from the reference mirror, respectively, toward a balanced 2 × 2 coupler connected to the detector, a 75 MHz bandwidth dual-channel balanced amplified photodetector (PDB 120C, Thorlabs). The detector output was digitized using a data acquisition card (ATS9462, AlazarTech) with 16-bit resolution and a sampling speed of 100 MS/s. In the acquired OCT images, the distance sampled per one unit of depth pixel is 6.25 μm.

The reference arm was terminated with a 14-mm diameter optical fiber collimator and a fixed flat mirror. Meanwhile, after the light in the sample arm propagated through the circulator and exited through an 8.4 mm diameter fiber collimator, it encountered a galvanometric system (6240 HM, Cambridge Technology) with two mirrors that scanned the sample beam across the entrance of a telecentric f-theta lens system (TSL-1550-80-195 Ronar-Smith) with an angular amplitude of ± 12°, which allowed for a multitude of scanning patterns across a region of interest. With a manufacturer-recommended working distance of 272 mm in the image plane, the telecentric system kept the probing beam parallel to its main optical axis while scanning across a maximum field of view of 8 cm × 8 cm. The beam scanning, signal detection and processing in this swept-source OCT system was controlled by a LabView program developed in-house. The operational wavelength chosen for the OCT prototype was 1545 nm to offer reasonable depth of penetration into skin. It is documented that OCT systems with longer operating wavelengths can probe deeper into biological tissue [18].

Animal model and data acquisition

Our burn model used 5-6-month-old female pigs. Both sides of the dorsal midline of the back were shaved with a number 40 clipper blade. After shaving, the skin was scrubbed with water to clean the areas that were later examined. Eight sites, each 30 mm in diameter, were marked on the cleaned dorsal surface of the back of each pig with an indelible pen. Four of the sites were located on the right side of the dorsal midline while the other four were located on the left side. Localized burn injuries of varying degree were created on four of the eight sites using a 30 mm diameter heated brass rod. The remaining four uninjured sites were used as controls. The location of all sites was determined so that each site had an independent blood supply. Accordingly, the sites were spaced with boundaries no less than 40 mm apart. The peri wound area where increased blood flow and edema in response to the injury could be expected to extend approximately 10 mm from the site of the wound.

It should also be noted that the total wound area was far less than 1% of the total body surface area (TBSA). This ensured that there were minimal systemic effects, such as circulatory and metabolic alterations, which typically follow larger burn injuries. The model described in this protocol was purposely designed to minimize systemic effects arising from burn injuries. It has been reported that burns covering less than 15% of the TBSA of an adult human are considered to have minor systemic effects, as long as full thickness burns represent less than 2% of this area.

The eight sites, which consist of four controls and four burns, were assigned in an alternating arrangement; the pattern would follow a burn – control – burn – control burn… sequence. Also, the locations of control and burn sites were selected in a random fashion for each pig to avoid any bias in the data related to location, vasculature or systemic response.

Burns were created by using 30-mm diameter circular brass rods pre-heated in 100°C boiling water and held in contact with the skin at one of the previously defined locations. In order to obtain burns of various degrees, the brass rod was in contact with the skin for 3, 12, 20 or 75 seconds. This procedure generated superficial, intermediate partial, intermediate deep and full thickness burns, respectively. The same contact times were used for the pre-determined control sites but with brass rod temperature equilibrated in water heated at the body temperature of the pig.

OCT data was acquired from control and burned sites before and immediately after application of the brass rod. Further data was acquired at time points of one, two and three hours after application of the brass rod. A standardized data collection procedure was established in order to ensure experimental repeatability of the measurements. This procedure included controlling the OCT system parameters, the positioning of the investigated tissue region relative to the collection telecentric lens in the sample arm as well as the timing of data acquisition relative to the breathing cycle of the animal.

A distance of 272 mm between the exit of the telecentric lens terminating the sample arm and the surface of the tissue ensured a beam with a spot size diameter of 50-μm at the surface of the tissue and a through focus distance (depth of focus) of about 4.5 mm [17]. Because the sample beam depth-of-focus was at least five times greater than the depths probed within the tissue, which were usually within the 400-800 μm range, the OCT probing beam can be regarded as collimated along the extent of the probed depths. This arrangement minimized the effect that a divergent sample beam could have on OCT signal intensity recorded along the probed depth within the sample. For all data recorded for the purpose of this work, the distance between two adjacent probed points on the skin surface was 50 μm. We considered this to be sufficient spatial resolution for clinical utility and placed emphasis on the ability to survey large areas of tissue, rapidly rather than on high spatial resolution.

Special care was exercised to minimize motion artifacts in the OCT data. In order to eliminate distortions induced by the periodic breathing movements of the animal, OCT data was acquired at the final stage of inhalation of the breathing cycle. At that moment the tissue surface was most stationary. The distance between the collector lens and the target tissue was adjusted so that, at the end of the inhalation cycle, the OCT image of the tissue surface was within the 150th to 200th depth pixel range, as exemplified in Figure 1. The design of our system also provided real-time viewing of the acquired OCT images during a scanning cycle thus enabling users to check the data acquisition quality and make operational adjustments to refine the quality of the OCT scans, if necessary. In addition, the depth (axial) resolution of this system (i.e. 6.25μm/depth pixel) allowed users to fine tune the position of the telecentric lens relative to tissue surface with a precision of 50 μm about the recommended work distance.

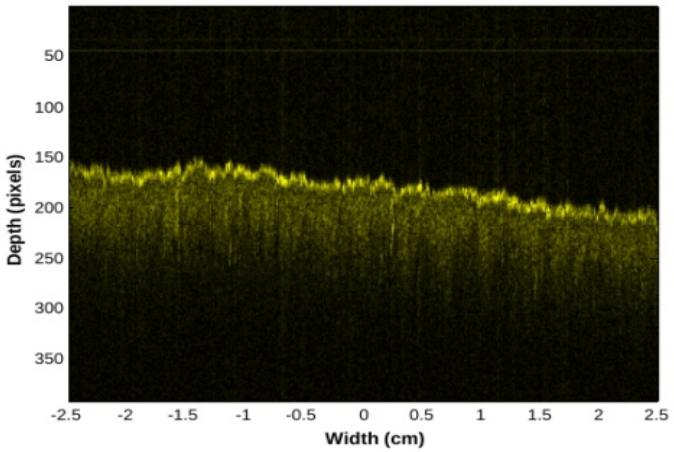

Figure 1. Example of an OCT image of pig skin acquired at the end of the inhalation stage of the breathing cycle. This image has a total 1,000 depth scans, with the distance between adjacent depth scans of 50 μm, thus corresponding to a sample width of 5 cm. One depth pixel unit corresponds to 6.25 μm

Figure 1 displays the type of OCT images of pig skin tissue that was acquired in this project. The image is composed of 1,000 depth scans at a 50 μm spacing, thus corresponding to a total scanned width of 5 cm on the sample. The tissue surface is displayed with a more intense shade of yellow due to the strong reflection of the probing beam at the air/skin interface. The light from the probing beam which passed through the skin surface propagated further inside the tissue and decreased gradually due to scattering and absorption. Meanwhile, the portion that was back-reflected and reached the detection after interference with light from the reference arm, generated the OCT signal corresponding to the probed location. The example shown in figure 1 displays an OCT signal back-reflected from the tissue surface down to approximately 600 μm under the skin surface.

The spotty pattern observed across the image shown in figure 1 is generated by coherent speckle noise. This type of noise is inherent to all imaging methods based on interference, including OCT. A consequence of this speckle is the very noisy profiles of individual depth scans. The speckle noise would not allow the calculation of a reliable attenuation coefficient for the OCT signal from individual depth scans. In order to obtain a smooth profile which would ensure a reliable estimation of an attenuation coefficient, we took advantage of the random character of the speckle noise and performed an averaging (compounding) of successive individual depth scans, thus generating a compounded profile. Before that we had to compensate for variations in the height of the sample surface. Thus, before the summation of depth scans, we applied a procedure for aligning the pixels corresponding to the reflection rise at the air/sample interface along a reference horizontal pixel line. The authors used and describe in detail the alignment and compounding procedures in another publication [19].

A total of seven animals were used in this acute, non-recovery protocol. The animals remained anesthetized through the entire protocol and were not recovered at the end. This protocol was approved by the animal care committee of the Institute for Bio diagnostics of the National Research Council of Canada. As described above, each specimen had eight pre-determined 30-mm diameter circular locations with 4 injury locations and 4 matching control locations. OCT data was acquired from all these locations before the application of burns, immediately after application of burns and 1, 2, and 3 hours after injury. Each image had the same specifications as the example provided in figure 1: composed of 1,000 depth scans, with distance between adjacent depth scans of 50 μm and imaging a total width of 5 cm across the region of interest. At each location we acquired two image sets, one immediately after the other, each set at a different position within the marked location. Each set contains six images, all acquired near or at the peak of the inhalation stage of the breathing cycle thereby minimizing motion artifacts. The speed of acquisition was a very important parameter in this study. Each image set (i.e. six images) was acquired in less than three seconds, and this interval included the time required to scan the region of interest with the probing beam, pre-process the data, display all six images and save data for future processing. Two images from each set were selected for analysis. The selected images had the imaged tissue surface in the range from the 150th to the 200th depth pixel. There were always cases when respiratory movements occurring during acquisition and/or the topography of the region of interest placed data portions from any set outside this optimal range. From each selected image, a group of two hundred successive depth scans, corresponding to a one-centimeter width from within a marked dorsal zone, were aligned and compounded. Subsequently, the marker for burn severity we wanted to test, the attenuation coefficient of OCT signal propagating inside the tissue was extracted from the compounded profile through an exponential fit.

Discussion

Figure 2 compares the OCT signal attenuation at control sites before and immediately after the application of brass rods heated at the specimen's body temperature. There is a small but statistically insignificant difference in the attenuation coefficients before and after the injury. This confirmed that there was not a large systemic response to the burn injury nor significant cross-talk between burn and control regions affecting the OCT signal at the control sites.

Figure 3 shows the average attenuation coefficients measured at all control and all burn sites over the full post-burn period (0 to 3 h). There was a statistically significant difference between the attenuation coefficients measured at the control and burn sites.

Figure 4 shows the evolution of attenuation coefficients at the burn and control sites over time, from moment 0 (immediately post-burn) to 3 h post-injury. The attenuation coefficients within both burn and control groups display no significant change over time but the two groups are statistically significantly different over the full post-burn period.

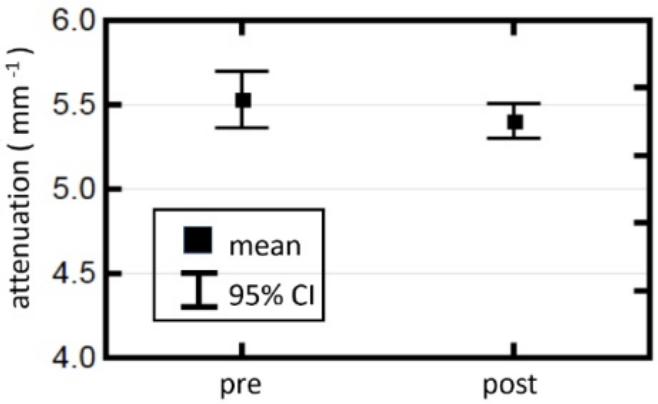

Figure 2. Comparison of attenuation coefficients measured in the control sites pre and post-injury

Figure 5 compares the OCT attenuation coefficients from the different burn types along with those of the control sites over the course of the protocol. None of the OCT attenuation coefficients show a significant temporal change during the 3-h time frame. No significant difference was observed between the OCT attenuation coefficients from the control sites (blue trace) and the 3 s injury (red trace). The 3 s injury was histologically confirmed to be confined to the epidermis and correspond to a superficial thickness injury. The 12 and 20 s injuries were histologically confirmed to result in partial thickness injuries. OCT coefficients from the sites of these injuries were significantly lower than those from control and 3 s injuries. Also, the two partial thickness injuries, 12 and 20 s, had significantly different OCT attenuation coefficients. The 75 s burn resulted in a full thickness injury and yielded significantly lower OCT attenuation coefficients (black trace) compared to the other more superficial injuries and the control sites.

Figure 6 plots the OCT attenuation coefficients from the different burn types along with the control sites pooling the measurements made over the early post-burn period (0 to 3 h). This plot more clearly shows the drop in the OCT attenuation coefficient with severity of the burn injury. The exception is the 3 s injury which shows no significant difference from the measurements made at the control sites. This can be rationalized by the superficial nature of the 3 s injury where only the epidermis is disrupted. As the injuries extend into the dermis the attenuation coefficient decreases in a manner consistent with the histological depth of the injury.

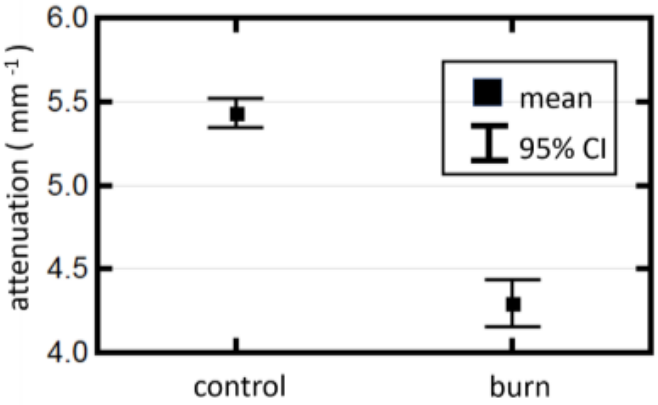

Figure 3. Comparison of attenuation coefficients from control and burn sites recorded over the full post-burn period of 3 h

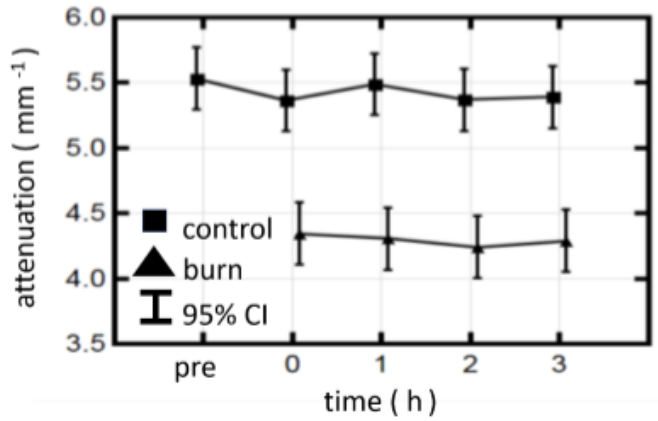

Figure 4. Evolution of attenuation coefficients from control and burn sites measured across the full post-burn period of 3 h

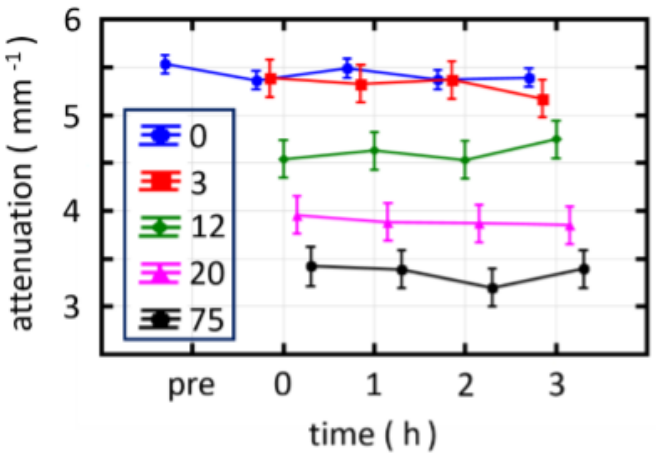

Figure 5. Evolution of groups of attenuation coefficients from control and burn sites separated by severity (burn application time length) measured across the full post-burn period of 3 h. The legend marked as "0" represents the control sites (i.e. zero seconds of burn contact)

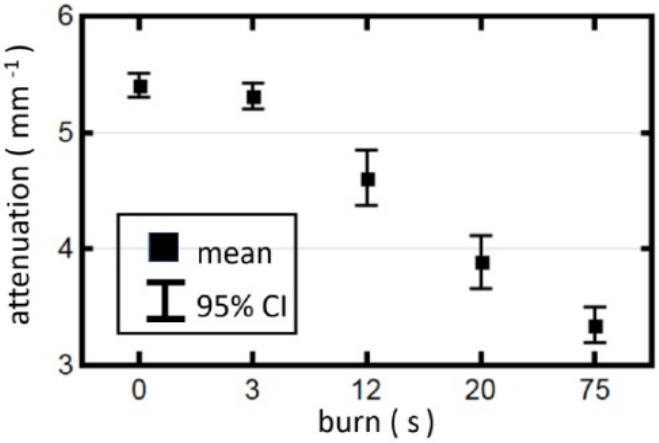

Figure 6. Attenuation coefficients for control and burn sites of different severities

Conclusion

A porcine burn model was used to evaluate the utility of a swept-source OCT prototype we designed and built specifically for deployment in burn trauma centers. A key feature of the OCT system that makes it suited to operating in that environment is the large stand-off distance between the instrument and the patient minimizing the risk of instrument borne wound contamination. Also paramount in the design specifications were the ability to scan large areas of tissue rapidly and to provide a near real-time assessment of the degree of injury without extensive image processing, segmentation or a subjective visual assessment of the OCT images. The OCT signal attenuation coefficient was used as a summary metric to provide an initial, non-subjective, real-time assessment of burn injury. Our model created contact burns of four different ranges of severity, superficial, superficial-partial, deep-partial and full thickness injuries. The model was a non-recovery, acute protocol where the animals remained anaesthetized over the duration of the protocol. The OCT signal attenuation coefficient was measured pre-injury, immediately post-injury, and at 1, 2 and 3-h post-injury. At the control sites there was no significant temporal change in the measured OCT attenuation coefficient. At the burn sites, post-injury, there was no significant change in the OCT attenuation coefficients between the immediate, 1, 2 and 3 h post injury measurements. Post-

injury there was no significant difference between the OCT attenuation coefficients measured at the control and superficial (3s-contact) injury sites. However, for all other burn types, superficial-partial, deep-partial and full thickness injuries, there was a significant difference in OCT attenuation from control. Additionally, significant differences were observed between the different types of burn injuries, superficial from superficial-partial from deep-partial from full thickness. The values of attenuation coefficients measured across this time interval presented a clear dependence on the burn severity. We can conclude that our OCT prototype using the OCT signal attenuation coefficient as a summary measure of burn injury has the potential for deployment in a burn trauma center to provide a rapid, non-contact means to survey large areas of tissue and provide an initial assessment of the degree of injury in the early post-burn period. Visual wound assessment in the early post-burn period is challenged and our approach could provide a useful adjunct to clinical assessment when it is the most in need of supporting information.

Acknowledgements

Funding was provided by Defense Research and Development Canada–Centre for Security Science (DRDC CSS) under the CRTI program. The authors would like to thank Bernhard Schattka, Mark Hewko, and Glen Kolansky for their engineering expertise in the development and deployment of the prototype OCT system. The authors would also like to thank the individuals who provided various other technical support for the project.

References

1. Heimbach D, Engrav L, Grube B, Marvin J (1992) Burn depth: A review. *World J Surg* 16: 10-15.
2. Jeng JC, Bridgeman A, Shivnan L, Thornton PM, Alam H, et al. (2003) Laser Doppler imaging determines need for excision and grafting in advance of clinical judgement: a prospective blinded trial. *Burns* 29: 665-670.
3. Pham TN, Gibran NS, Heimback DM (2002) Evaluation of the burn wound: management decisions, in Total Burn Care, ed. D. Herndon, Edinburgh: Saunders, pp: 119-126.
4. Desai MH, Rutan RL, Herndon DN (1991) Conservative Treatment of Scald Burns Is Superior to Early Excision. *J Burn Care Rehabil* 12: 482-484.
5. Foglia RP, Moushey R, Meadows L, Seigel J, Smith M, et al. (2004) Evolving treatment in a decade of pediatric burn care. *J Pediatr Surg* 39: 957-960.
6. Sainsbury DC (2008) Critical evaluation of the clinimetrics of laser Doppler imaging in burn assessment. *J Wound Care* 17: 193-194.
7. McGill DJ, Sorensen K, MacKay IR, Taggart I, Watson SB (2007) Assessment of burn depth: a prospective, blinded comparison of laser Doppler imaging and videomicroscopy. *Burns* 33: 833-842.
8. Waxman K, Lefcourt N, Achauer B (1989) Heated laser Doppler flow measurements to determine depth of burn injury. *Am J Surg* 157: 541-543.
9. Holland AJ, Ward D, Farrell B (2007) The influence of burn wound dressings on laser Doppler imaging assessment of a standardized cutaneous injury model. *J Burn Care Res* 28: 871-878.
10. Jerath MR, Schomacker KT, Sheridan RL, Nishioka NS (1999) Burn wound assessment in porcine skin using indocyanine green fluorescence. *J Trauma* 46: 1085-1088.
11. Kamolz LP, Andel H, Haslik W, Donner A, Winter W, et al. (2003) Indocyanine green video angiographies help to identify burns requiring operation. *Burns* 29: 785-791. [Crossref]
12. Benya R, Quintana J, Brundage B (1989) Adverse reactions to indocyanine green: a case report and a review of the literature. *Cathet Cardiovasc Diagn* 17: 231-233.
13. Sowa MG, Leonardi L, Payette JR, Cross KM, Gomez M, et al. (2006) Classification of burn injuries using near-infrared spectroscopy. *J Biomed Opt* 11: 054002.
14. Weingarten MS, Papazoglou ES, Zubkov L, Zhu L, Neidrauer M, et al. (2008) Correlation of near infrared absorption and diffuse reflectance spectroscopy scattering with tissue neovascularization and collagen concentration in a diabetic rat wound healing model. *Wound Repair Regen* 16: 234-242.
15. Sowa MG, Leonardi L, Payette JR, Fish JS, Mantsch HH, et al. (2001) Near infrared spectroscopic assessment of hemodynamic changes in the early post-burn period. *Burns* 27: 241-249.
16. Ross KM, Leonardi L, Payette JR, Gomez M, Levasseur MA, et al. (2007) Clinical utilization of near-infrared spectroscopy devices for burn depth assessment. *Wound Repair Regen* 15: 332-340.
17. Popescu DP, Smith MSD, Sowa MG (2014) Characterization of Optical Coherence Tomography Images Acquired At large Distances with Large-Diameter Beams. *IEEE Photonics J* 6: 1-11.
18. Kodach V, Kalkman J, Faber D, Van Leeuwen T (2010) Quantitative comparison of the OCT imaging depth at 1300 nm and 1600 nm. *Biomed Opt Express* 1: 176-185. [Crossref]
19. Popescu DP, Sowa MG, Hewko MD, Choo-Smith LP (2008) Assessment of early demineralization in teeth using the signal attenuation in optical coherence tomography images. *J Biomed Opt* 13: 054053. [Crossref]